

The ratio of $\Psi(2s)$ and J/Ψ exclusive photoproduction cross-sections as a tool to detect non-linear QCD evolution

Marco Antonio Alcazar Peredo¹ and Martin Hentschinski²

¹*Instituto de Física Teórica, Universidad Autónoma de Madrid, 28049 Madrid, Spain*

²*Departamento de Actuaría, Física y Matemáticas, Universidad de las Américas Puebla, Santa Catarina Martir, 72820 Puebla, Mexico*



We study the proposal that the rise with energy of the ratio of $\Psi(2s)$ and J/Ψ exclusive photoproduction cross-sections might serve as an indicator of the presence of non-linear QCD evolution, related to the presence of high and potentially saturated gluon densities in both the proton and a lead nucleus. Our study employs recent fits of the GBW and BGK dipole models and provides predictions for both exclusive photoproduction on a proton and on a lead nucleus. While the cross-sections for photoproduction on a proton depend only weakly on non-linear low x corrections, we find an increased sensitivity for the cross-section ratio, which is directly related to the node in the $\Psi(2s)$ wave function. We further give a description of recent ALICE data for exclusive J/Ψ photoproduction on a lead nucleus and provide predictions for $\Psi(2s)$ photoproduction on a lead nucleus as well as for the corresponding cross-section ratio.

DOI: <https://doi.org/10.17161/8cyw5q54>

Keywords: Diffractive production, QCD phenomenology, Quantum chromodynamics, Strong interaction

1 Introduction

Exclusive photoproduction of charmonium in ultra-peripheral collisions at the Large Hadron Collider (LHC) provides a unique opportunity to examine Quantum Chromodynamics (QCD) at very low values of x . With $x = M_V^2/W^2$, where M_V is the mass of the vector meson, and W the center-of-mass energy of the photon-proton or photon-nucleus collision, this corresponds to the high-energy limit of perturbative strong interactions. Examining this low x limit is of interest, since it allows us to investigate an important open question in the exploration of strongly interacting matter: In the above-described interaction of a photon with a proton (or an entire nucleus), we explore the gluon distribution of the proton (or nucleus), if the reaction occurs in the presence of hard scale; the latter allows for the identification of partonic degrees of freedom. Such a scenario is realized for charmonium production, where the mass of the charm quark provides the hard mass scale. In the region of phase space where the variable x takes small values – roughly speaking values smaller than 0.01 – BFKL evolution predicts for the inclusive gluon distribution a powerlike rise with x . While such a rise has been clearly seen in data, there are strong theoretical arguments that suggest that such a rise must at some value of x slow down and eventually come to hold^{1,2}. The growth of the gluon density will therefore saturate at some value of x . While there are strong arguments for gluon saturation, the determination of the value of x , where this new phenomena should manifest itself in data, is still an open task.

Reactions that involve charmed final states are in this context particularly interesting^{3,4}, since they sit on the boundary between perturbative and non-perturbative QCD dynamics. While the presence of a hard scale is essential for a description based on microscopic degrees of freedom, a large hard scale will select regions of the phase space, where non-linear terms in QCD evolution equations are suppressed. These

non-linear terms occur in extensions of the BFKL evolution equation, such as the BK equation, where they lead to a slowdown of the growth of the gluon distribution. Previously, a description of the energy dependence of the photoproduction cross-sections of charmonium^{5,6,7,8,9,10,11} has been provided through comparing fits of unintegrated gluon distributions subject to next-to-leading order (NLO) BFKL evolution^{12,13,14} (Hentschinski-Salas-Sabio-Vera; HSS) and DGLAP-modified BK evolution¹⁵ (Kutak-Sapeta; KS). This approach allows for direct evaluation of linear and non-linear low- x frameworks and attempts to search for features which distinguish between them, if compared to experimental data. Although unintegrated gluon distributions subject to linear and non-linear QCD evolution start to diverge at values of $x < 10^{-4} - 10^{-5}$, uncertainties prevent drawing firm conclusions whether signs of non-linear QCD dynamics are present in data. However, it was noted^{8,5} that the ratio of photoproduction cross-sections of $\Psi(2s)$ and J/Ψ vector mesons shows distinct energy dependence for linear (BFKL) and non-linear (BK) evolution equations: The ratio rises with energy under full non-linear QCD evolution, while it stays relatively constant with linear evolution. Although the rise in the ratio of $\Psi(2s)$ and J/Ψ photoproduction cross-sections with energy has been previously documented for unitarized dipole models^{16,17}, the constant ratio with linear QCD evolution has not been thoroughly studied, to the best of our knowledge.

An interesting question in this context is whether the observed features are a coincidence related to the specific form of the HSS and KS distributions or whether they constitute a general characteristic of dipole cross-sections and/or gluon distributions with or without non-linear QCD dynamics. We therefore repeat the previous analysis⁵, using two dipole models to represent the gluon density: the Golec-Biernat Wusthoff⁸ (GBW) and the Bartels Golec-Biernat Kowalski⁷ (BGK) model. While these are models which themselves are not subject to low x QCD evolution equations, they allow for direct manipulation of non-linear corrections and therefore for an exploration of their relevance for the photoproduction cross-section. We work with both models in their linearized and complete exponentiated (unitarized) versions, offering detailed definitions further down. While our primary focus is on the ratio of $\Psi(2s)$ to J/Ψ photoproduction in photon-proton collisions, we also discuss recent data from the ALICE experiment on J/Ψ photoproduction in photon-lead collisions^{19,20}, using these models for our analysis. Additionally, we provide predictions for $\Psi(2s)$ photoproduction in photonuclear reactions and the ratio of $\Psi(2s)$ to J/Ψ .

In this contribution, we summarize essential recent results^{21,22}, to which refer the interested reader for more details.

2 Photoproduction cross-sections

We study the process,

$$\gamma(q) + H(p) \rightarrow V(q') + p(p'), \quad V = J/\Psi, \psi(2S), \quad (1)$$

where γ denotes a quasi-real photon with virtuality $Q \simeq 0$, which stems from an electron (HERA) or a proton/lead nucleus in the case of LHC data; H is the proton or lead nucleus respectively. $W^2 = (q+p)^2$ the squared center-of-mass energy of the $\gamma(q) + H(p)$ reaction. With $t = (q-q')^2$, the differential cross-section for the exclusive photo-production of a vector meson can be written as,

$$\frac{d\sigma}{dt}(\gamma p \rightarrow V p) = \frac{1}{16\pi} \left| \mathcal{A}_T^{\gamma p \rightarrow V p}(x, t) \right|^2, \quad V = J/\Psi, \psi(2S). \quad (2)$$

Here $\mathcal{A}_T(W^2, t)$ denotes the scattering amplitude for a transverse polarized real photon with color singlet exchange in the t -channel, with an overall factor W^2 already extracted. $x = M_V^2/W^2$ with M_V the mass of the vector meson⁷. We finally have for the photoproduction cross-section

$$\sigma^{\gamma p \rightarrow V p}(W^2) = \frac{1}{B_D(W)} \left. \frac{d\sigma}{dt}(\gamma p \rightarrow V p) \right|_{t=0}, \quad (3)$$

where B_D is diffractive slope parameter²¹. For the proton, we use¹⁷

$$B_{D,p}(W) = \left[b_{0,p} + 4\alpha'_p \ln \frac{W}{W_0} \right] \text{GeV}^{-2}, \quad (4)$$

with $b_{0,p}^{J/\Psi} = 4.62$, $b_{0,p}^{\Psi(2s)} = 4.86$, $\alpha'_p{}^{J/\Psi} = 0.171$ and $\alpha'_p{}^{\Psi(2s)} = 0.151$. For the lead nucleus we have $B_D = (4.01 \pm 0.15) \cdot 10^2/\text{GeV}^2$, which we determined from a fit to the $|t|$ dependence of the coherent J/Ψ photonuclear production by the ALICE collaboration²³.

2.1 Wavefunction overlap

Within high energy factorization, the imaginary part of the scattering amplitude at $t = 0$ is obtained as a convolution of the light-front wave function – which describes the formation of a color dipole and its subsequent transition into a vector meson – and the dipole cross-section. In the following, we use a simple Gaussian model for the vector meson wave function,

$$\Im \mathcal{A}_T^{\gamma p \rightarrow V p}(x, t = 0) = \int d^2\mathbf{r} \Sigma(r) \sigma_{q\bar{q}}(x, r), \quad (5)$$

where $r = |\mathbf{r}|$ denotes the transverse separation of the dipole and

$$\begin{aligned} \Sigma(r) &= \int_0^1 \frac{dz}{4\pi} (\Psi_V^* \Psi_T)(r, z) \\ &= \int_0^1 \frac{dz}{4\pi} \frac{\hat{e}_f e N_c}{\pi z(1-z)} \left\{ m_f^2 K_0(m_c r) \phi_T(r, z) - [z^2 + (1-z)^2] \epsilon K_1(m_c r) \partial_r \phi_T(r, z) \right\}. \end{aligned} \quad (6)$$

Although previously⁵ a more refined description of the wave function overlap^{24,17} has been used, the effects are minimal for our current study. Thus, we opted for the simpler boosted Gaussian model following the Brodsky-Huang-Lepage prescription^{25,7,7}:

$$\phi_T^{1s}(r, z) = \mathcal{N}_{T,1s} z(1-z) \exp\left(-\frac{m_f^2 \mathcal{R}_{1s}^2}{8z(1-z)} - \frac{2z(1-z)r^2}{\mathcal{R}_{1s}^2} + \frac{m_f^2 \mathcal{R}_{1s}^2}{2}\right), \quad (7)$$

$$\begin{aligned} \phi_{T,L}^{2s}(r, z) &= \mathcal{N}_{T,2s} z(1-z) \exp\left(-\frac{m_f^2 \mathcal{R}_{2s}^2}{8z(1-z)} - \frac{2z(1-z)r^2}{\mathcal{R}_{2s}^2} + \frac{m_f^2 \mathcal{R}_{2s}^2}{2}\right) \\ &\cdot \left[1 + \alpha_{2s} \left(2 + \frac{m_f^2 \mathcal{R}_{2s}^2}{4z(1-z)} - \frac{4z(1-z)r^2}{\mathcal{R}_{2s}^2} - m_f^2 \mathcal{R}_{2s}^2 \right) \right]. \end{aligned} \quad (8)$$

The free parameters of this parametrization have been determined in various studies from the normalization and orthogonality of the wave functions as well as the decay width of the vector mesons. Here we use²⁶ $\mathcal{N}_{T,1s} = 0.57$, $\mathcal{N}_{T,2s} = 0.67$, $m_c = 1.4$ GeV, $\mathcal{R}_{1s}^2 = 2.45$ GeV⁻², $\mathcal{R}_{2s}^2 = 3.72$ GeV⁻², $\alpha_{2s} = -0.61$ and $m_c = 1.4$ GeV.

2.2 Dipole cross-sections

Within collinear factorization, one finds to leading order for the dipole cross-section^{27 28}

$$\sigma_{q\bar{q}}^{\text{collinear}}(x, r) = \frac{\pi^2}{3} r^2 \alpha_s(\mu^2) x g(x, \mu^2). \quad (9)$$

The renormalization scale μ is usually identified with the factorization scale and taken to depend on the dipole size with $\mu^2 \sim 1/r^2$ for small dipole sizes; $xg(x, \mu^2)$ denotes the collinear gluon distribution subject to leading order DGLAP evolution. A simple way to estimate corrections that yield unitarization of this dipole cross-section in the limit of large dipole separations r and/or large gluon densities is to exponentiate the collinear cross-section, which yields the Bartels–Golec-Biernat–Kowalski (BGK) model,

$$\sigma_{q\bar{q}}^{\text{BGK}}(x, r) = \sigma_0^{\text{BGK}} \left[1 - \exp\left(-\frac{r^2 \pi^2 \alpha_s(\mu_r^2) x g(x, \mu_r^2)}{3\sigma_0^{\text{BGK}}}\right) \right]. \quad (10)$$

The above exponentiation introduces a new parameter, σ_0 , which yields the value of the dipole cross-section in the black disk limit, corresponding to the transverse size of the target. An even simpler model is provided by the Golec-Biernat, Wüsthoff (GBW) model,

$$\sigma_{q\bar{q}}^{\text{GBW}}(x, r) = \sigma_0^{\text{GBW}} \left[1 - \exp\left(-\frac{r^2 Q_s^2(x)}{4}\right) \right], \quad Q_s^2(x) = Q_0^2 \left(\frac{x_0}{x}\right)^\lambda, \quad (11)$$

where Q_s denotes the saturation scale within the model and gathers various elements of the collinear cross-section into a single factor. Both models have been recently refitted for dipole scattering on a proton to combined HERA data in²⁹ where free parameters are obtained as $\sigma_0^{\text{GBW}} = (27.43 \pm 0.35)$ mb,

$\lambda = 0.248 \pm 0.002$, $x_0 = (0.40 \pm 0.04) \cdot 10^{-4}$, while $Q_0 = 1$ GeV for the GBW model. For the BGK model, $g(x, \mu^2)$ is subject to leading order DGLAP evolution equation without quarks,

$$\frac{d}{d\mu^2}g(x, \mu^2) = \frac{\alpha_s}{2\pi} \int_x^1 \frac{dz}{z} P_{gg}(z)g(x/z, \mu^2), \quad xg(x, Q_0^2) = A_g x^{-\lambda_g} (1-x)^{5.6}, \quad (12)$$

where $xg(x, Q_0^2)$ denotes the gluon distribution at the initial scale $Q_0 = 1$ GeV. Following the recent fit²⁹ of this model, we evaluate the gluon distribution and the QCD running coupling at the dipole size dependent scale

$$\mu_r^2 = \frac{\mu_0^2}{1 - \exp(-\mu_0^2 r^2/C)}. \quad (13)$$

The remaining parameters of the model have been obtained as $\sigma_0^{\text{BGK}} = (22.93 \pm 0.27)$ mb, $A_g = 1.07 \pm 0.13$, $\lambda_g = 0.11 \pm 0.03$, $C = 0.27 \pm 0.04$, $\mu_0^2 = (1.74 \pm 0.16)$ GeV². The exponentiated terms allow us within these simple models to explore the relevance of non-linear QCD dynamics for the description of data.

2.3 Modified Dipole Cross-sections and nuclear effects

To explore the relevance of the exponentiated terms, which simulate non-linear QCD evolution, we will compare for the following numerical study both complete and linearized models. In addition, we introduce in the following a parameter ‘ k ’ which allows for a smooth transition between both scenarios, i.e., which allows to vary the ‘density’ of gluons by hand. We introduce this parameter k through a rescaling $Q_s^2(x) \rightarrow k \cdot Q_s^2(x)$, while we keep the linearized dipole cross-sections fixed. For the GBW model, this leads to

$$\begin{aligned} \sigma_{q\bar{q}}^{\text{GBW}}(x, r, k) &= \sigma_0^{\text{GBW}} Q_s^2(x) \left(\frac{r^2}{4}\right) \left[1 + \sum_{n=1}^{\infty} \frac{1}{(n+1)!} \left(-k \cdot \frac{r^2 Q_s^2(x)}{4}\right)^n\right] \\ &= \frac{\sigma_0^{\text{GBW}}}{k} \left[1 - \exp\left(-k \cdot \frac{r^2 Q_s^2(x)}{4}\right)\right]. \end{aligned} \quad (14)$$

With this modification, $k = 0$ corresponds to the linear case, whereas $k = 1$ yields the current HERA fit of the model; finally, $k > 1$ implies an additional enhancement of non-linear effects. Within this simple approach, k can be understood as a parameter that controls the strength of the triple Pomeron vertex and, therefore, the relevance of non-linear dynamics. We also apply an identical modification to the BGK model,

$$\sigma_{q\bar{q}}^{\text{BGK}}(x, r, k) = \frac{\sigma_0^{\text{BGK}}}{k} \left[1 - \exp\left(-k \cdot \frac{r^2 \pi^2 \alpha_s(\mu_r^2) xg(x, \mu_r^2)}{3\sigma_0^{\text{BGK}}}\right)\right]. \quad (15)$$

If the color dipole scatters on a large nucleus instead of a single proton, one expects an increase in the saturation scale due to the nuclear ‘‘oomph factor’’,

$$Q_{s,A}^2(x) \simeq A^{\frac{1}{3}} Q_s^2(x), \quad (16)$$

where A denotes the number of nucleons in the nucleus, and $Q_{s,A}^2(x)$ is the saturation scale for the nuclear target, while $Q_s^2(x)$ denotes the saturation scale for a single proton, as obtained from the fit to HERA data. With the transverse size of the dipole cross-section scaling as $\sim A^{2/3}$, we finally obtain

$$\sigma_{q\bar{q},A}(x, r) = A^{\frac{2}{3}} \sigma_{q\bar{q}}(x, r, k = A^{\frac{1}{3}}). \quad (17)$$

3 Non-linear corrections and the $\Psi(2s)$ over J/Ψ ratio

Having set up the theoretical framework, we ask ourselves the question whether one can expect a manifestation of non-linear QCD dynamics in the photoproduction of J/Ψ and $\Psi(2s)$ vector mesons. Taking a first look at the predictions for the production cross-section, Fig. 1, we observe a clear difference between linearized and complete dipole models. Compared to the results based on BFKL/BK evolution⁵, one observes that the difference between linear and non-linear cases is more pronounced in the case of dipole models. This is not a surprise: while both HSS (linear) and KS (non-linear) gluon distributions

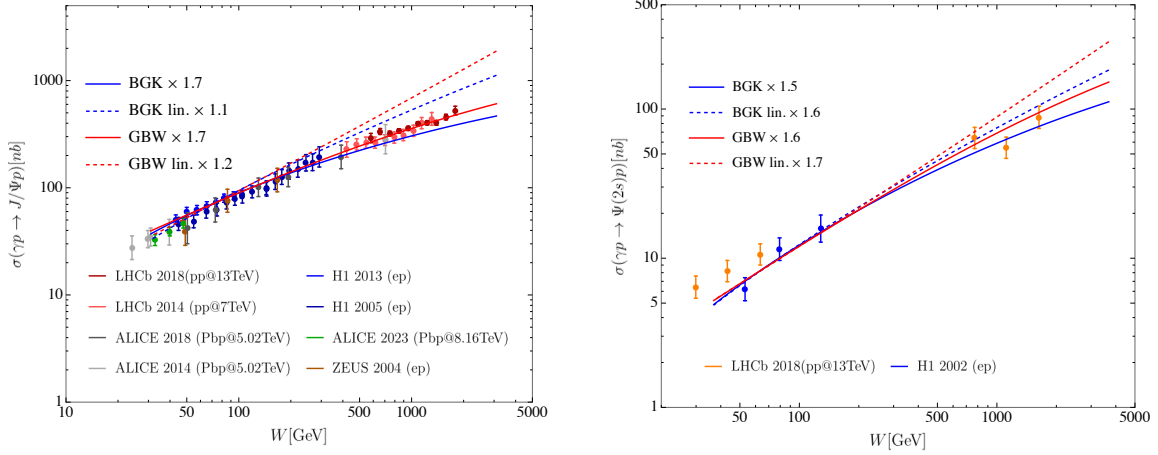


Figure 1 – Energy dependence of the total cross-sections for exclusive photoproduction of J/Ψ (left) and $\Psi(2s)$ (right) as obtained within the dipole models discussed in the text. We further display photo-production data measured at HERA by ZEUS³⁰ and H1^{31,32} collaborations as well as LHC data obtained from ALICE^{33,34,35} and LHCb^{36,37} for J/Ψ production as well as H1^{38,39} and LHCb data³⁷ for the $\Psi(2s)$ photoproduction cross-section.

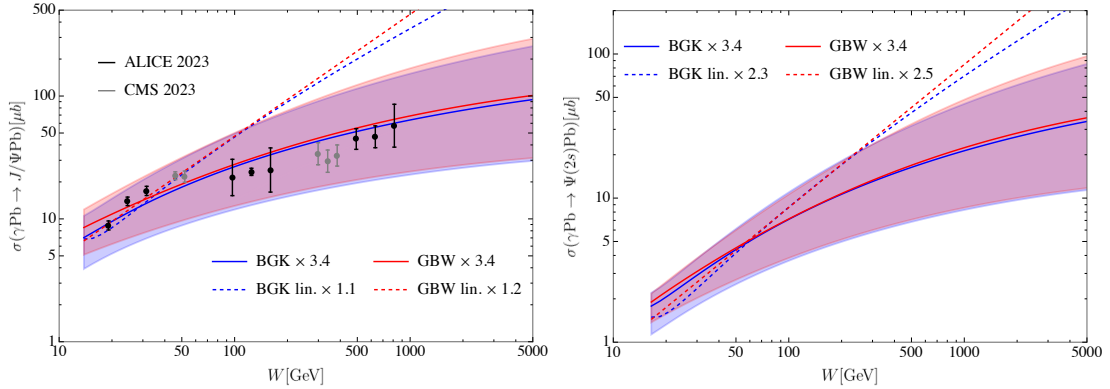


Figure 2 – Predictions of the photonuclear production of J/Ψ and $\Psi(2s)$. We further show ALICE¹⁹ and CMS⁴⁰ data.

have been fit to HERA data, for the dipole models such a fit has been only performed for the complete (non-linear) models. This is also the reason why we require different K-factors for linearized and complete models. Fig. 2 provides the corresponding predictions for the photonuclear reaction, where charmonium is produced through the scattering of a photon on a lead nucleus. In comparison to the proton case, the energy dependence of the complete dipole models shows now a clear saturation effect in the sense that there is a clear difference between the powerlike rise with the energy of the linearized models and the energy dependence of the complete models. We however note that the energy dependence of the linearized model is identical to the energy dependence of the proton cross-section; nuclear shadowing effects absent in this case. As discussed in¹⁹, the data set can be described with a similar accuracy if one employs a powerlike growth, with a reduced Pomeron intercept. We believe that a closer investigation of this aspect would be a very interesting research task for the future.

3.1 Charmonium production and the scaling region

In the following, we would like to reinvestigate the potential relevance of non-linear corrections based on general estimates of the size of such corrections for different regions of phase space of the dipole cross-section. With

$$Q_s^{\text{GBW}}(x = 10^{-6}) \simeq 1.58 \text{ GeV}, \quad (18)$$

the numerical value of the saturation scale in the proton is close to the hard scale of the charmonium production cross-section, $m_c \simeq 1.4 \text{ GeV}$. One therefore does not enter a region of phase space where $Q_s^2 \gg m_c^2$ and where therefore an expansion of the cross-section in powers of Q_s^2/m_c^2 is clearly breaking

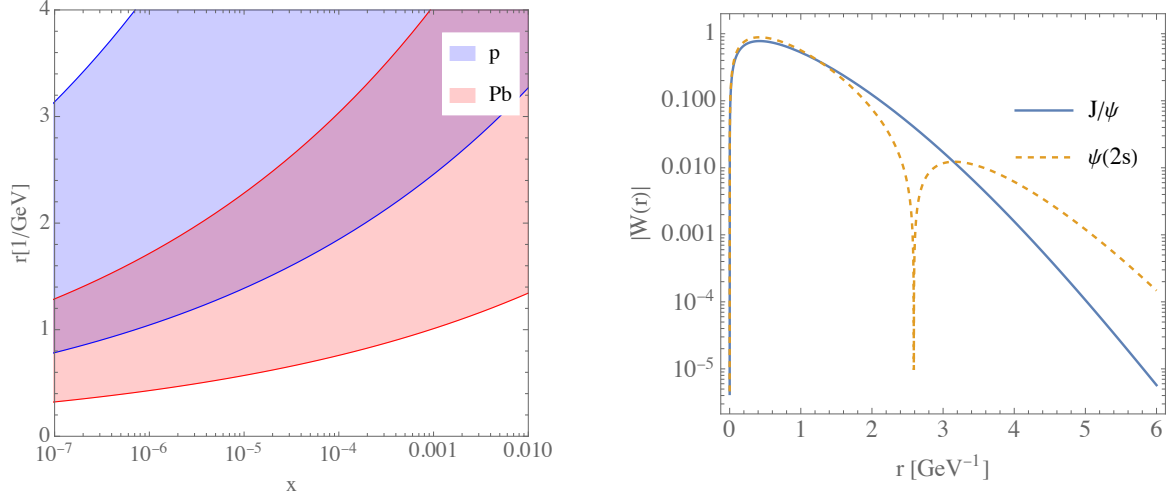


Figure 3 – Left: Estimated geometric scaling region, based on the GBW saturation scale for both proton and lead. Right: Integrated Gaussian wave function overlap for photo-production of vector mesons J/Ψ and $\Psi(2s)$

down. We are therefore not sensitive to the saturated region of the dipole cross-section, but at most to the so-called (geometric) scaling region⁴¹. In this region of phase space, the dimensionless dipole cross-section $\sigma_{q\bar{q}}(x, r)/\sigma_0$ is still weak, $\sigma_{q\bar{q}}(x, r)/\sigma_0 \ll 1$, but the existence of a region of saturated dipole cross-section⁴² $\sigma_{q\bar{q}}(x, r)/\sigma_0 \sim 1$ reflects itself already in the dynamics of the dipole cross-section. Seen from a different perspective, the geometric scaling region can be defined as the range in dipole size r , where the dipole cross-section $\sigma_{q\bar{q}}(x, r)$ turns into a function of a single variable, $\sigma_{q\bar{q}}(x, r) \rightarrow \sigma_{q\bar{q}}(r^2 Q_s^2(x))$; the saturation scale therefore turns in this region of phase space into the relevant mass scale of the dipole cross-section. Note that such a dependence is generally assumed in the employed dipole models.

Using properties of solutions to the BK equations, this scaling region can be estimated using the following inequality^{43,44,45}:

$$1 < |\ln(r^2 Q_s^2(x))| \leq \sqrt{\bar{\alpha}_s \chi_0''(\gamma_0)}, \quad (19)$$

with $\chi_0(\gamma) = 2\Psi(1) - \Psi(\gamma) - \Psi(1 - \gamma)$ the leading order BFKL eigenvalue and γ_0 implicitly defined through $\chi_0(\gamma_0)/\gamma_0 = \chi_0'(\gamma_0)$ with $\gamma_0 \simeq 0.627549$. The resulting scaling region is illustrated in Fig. 3 (left) using the GBW saturation scale and $\bar{\alpha}_s(m_c) \simeq 0.29$, for both the proton and a lead nucleus. For the proton, even at the lowest accessible values of x , one enters the scaling region only for $r > 1/\text{GeV}$; one is therefore in a region of phase space which is dominated by non-perturbative dynamics. This is in general one of the reasons why one searches for events on the boundary between perturbative and non-perturbative QCD dynamics, since it is this region of phase space where non-linear effects are enhanced. For a lead nucleus, the scaling region starts already at $r > 0.4/\text{GeV}$, since the gluon density is enhanced through the overlap of various nucleons. To compare the scaling region to the region in dipole sizes probed for J/Ψ and $\Psi(2s)$ production, we introduce the normalized wave function overlap

$$W_V(r) = \frac{r \int_0^1 dz (\Psi_V^* \Psi_T)(r, z)}{\int dr r \int_0^1 dz (\Psi_V^* \Psi_T)(r, z)}, \quad \int_0^\infty dr W(r) = 1, \quad (20)$$

see Fig. 3, right; note that $W_{\Psi(2s)}(r) < 0$ for $r > 2.59/\text{GeV}$. To access the relevance of the different regions in dipole size r for the complete cross-section, we further provide in Tab. 1 the integrated $W_V(r)$ function for different regions. For the photonuclear production cross-section, the bulk of the dipole sizes probed in the reaction – approximately three quarters – lies within the geometric scaling region; this

Table 1: Percentage of $w_V = \int_{r_{min}}^{r_{max}} dr W_{J/\Psi}$ for different regions of dipole size r . Note that the $W_{\Psi(2s)} < 0$ for $r > 2.59/\text{GeV}$.

	$0 < r < 0.4/\text{GeV}$	$0.4 < r < 1/\text{GeV}$	$1 < r < 3/\text{GeV}$	$r > 3/\text{GeV}$
$w_{J/\Psi}(\%)$	23.6	40.8	34.9	0.7
$w_{\Psi(2s)}(\%)$	26.7	45.7	30.0	- 1.4

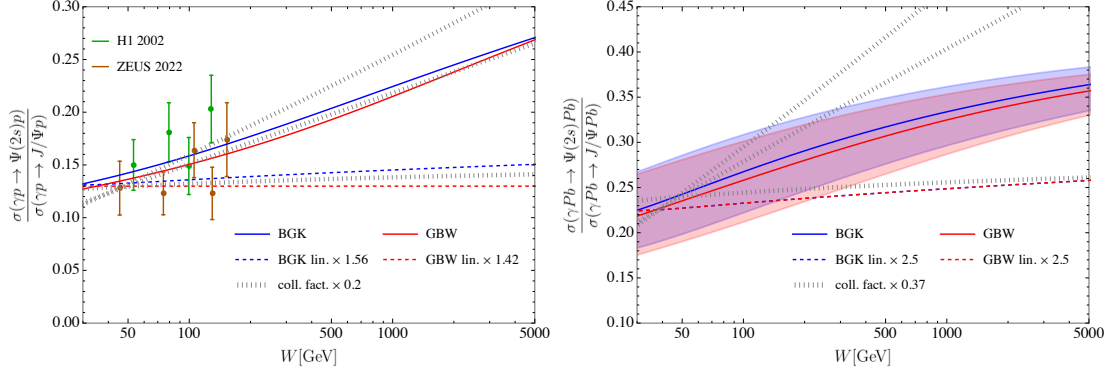


Figure 4 – Ratio of photoproduction cross-sections both for the proton (left) and lead (right). For the proton we further depict ZEUS⁴⁶ and H1⁴⁷ data

explains the clear imprint of a non-linear energy dependence in the photoproduction cross-section shown in Fig. 2. For photoproduction on a proton, this contribution is however reduced to approximately a third, which explains the relatively weak non-linear dynamics in Fig. 1.

3.2 The ratio of the photo-production cross-sections

To have access to the geometrical scaling region in the proton, it is necessary to probe observables that are somehow sensitive to dipole sizes $1 < r < 3/\text{GeV}$. In this region, both wave function overlaps are still sizeable, while they differ significantly in shape due to the node of $W_{\psi(2s)}$ at $r = 2.59/\text{GeV}$. A possibility to gain sensitivity to this region is given by observables which attempt to probe the difference in this wave function shape. An obvious candidate is obviously the ratio of both photo-production cross-sections. To understand the behavior of this ratio, it is best to study it first for the scenario where non-linear dynamics are absent. For the linearized GBW model,

$$\sigma_{q\bar{q}}^{\text{GBW, lin.}}(x, r) = \sigma_0^{\text{GBW}} r^2 Q_s^2(x)/4, \quad (21)$$

Eq. (5) turns into

$$\Im \mathcal{A}_T^{\gamma p \rightarrow V p}(x) = Q_s^2(x) \cdot \sigma_0^{\text{GBW}} \int d^2 \mathbf{r} \Sigma(r) r^2 / 4, \quad V = J/\Psi, \Psi(2s). \quad (22)$$

For the ratio of both photoproduction cross-sections, the energy dependence therefore cancels and one is left with a ratio constant with energy. This differs for the complete dipole model, where x and r -dependence do not factorize. For the BGK model, one finds a dipole size dependent saturation scale or gluon distribution. The x -dependence does therefore not cancel in the ratio. Nevertheless, in the region of interest corresponding to dipole sizes $r > 1/\text{GeV}$, the factorization scale approaches rapidly $\mu_0 \simeq 1.32 \text{ GeV}$ and one deals again with a dipole size independent saturation scale. For $r > 1/\text{GeV}$, the x -dependence of the collinear leading order dipole cross-section Eq. (9) turns r -independent and one finds again a ratio which is approximately x independent, if one sticks to the linear dipole cross-section. For $r < 1/\text{GeV}$, there is clearly a dependence on the dipole size, while in this region the shape of both wave functions is very similar; the difference will therefore not manifest itself at the cross-section level.

4 Predictions for the ratio of photoproduction cross-sections

We finally present our numerical results at the level of cross-sections measured in experiment in Fig. 4. As expected we find for the photoproduction on a proton an approximately linear growth of the cross-section ratio, if non-linear effects are fully included; the regarding linearized versions lead on the other hand to a cross-section ratio constant with energy W . The scenario is similar for photoproduction on a lead nucleus, with the important difference that for the largest center of mass energies we can already observe a slowdown of the growth of the ratio. This is in a certain sense a deviation from a possible growth of the ratio within collinear factorization, which can accommodate, but not predict a growing ratio. In that case, a growing or constant ratio is obtained due to different choices for the collinear factorization scale; for a detailed discussion we refer to the paper²¹.

5 Conclusions

We examined the proposal⁵, suggesting that an increasing ratio of photoproduction cross-sections for $\Psi(2s)$ and J/Ψ can be an indicator for non-linear low x dynamics in protons or nuclei. Our analysis utilized dipole cross-sections from the GBW and BGK models, which essentially exponentiate linear cross-sections to investigate the effects of non-linear low x dynamics. As an initial outcome, we confirmed that the observation⁵ holds if gluon distributions under linear NLO BFKL and non-linear BK evolutions are replaced by linearized and unitarized dipole models: without non-linear low x dynamics, the ratio of the two cross-sections remains nearly constant, but it rises when using the fully exponentiated dipole model. This behavior can be explained by the convolution of the dipole cross-section and the wave function overlap: if the dipole cross-section's shape changes with x in regions where wave function overlaps for the transition from photon to $\Psi(2s)$ and J/Ψ differ, the ratio increases. In linearized models, this phenomenon is absent because only the normalization changes with x while the shape in dipole size remains approximately constant, apart from minor adjustments from DGLAP evolution.

Acknowledgments

We acknowledge support by Consejo Nacional de Ciencia y Tecnología grant number A1 S-43940 (CONACYT-SEP Ciencias Básicas). We would like to thank Heikki Mäntysaari for pointing out to us the incorrect use of incoherent instead of coherent photonuclear ALICE data for the determination of the nuclear diffractive slope in our initial manuscript.

References

1. L.V. Gribov, E.M. Levin, and M.G. Ryskin. Semihard Processes in QCD. *Phys. Rept.*, 100:1–150, 1983.
2. Martin Hentschinski et al. White Paper on Forward Physics, BFKL, Saturation Physics and Diffraction. *Acta Phys. Polon. B*, 54(3):3–A2, 2023.
3. Francesco Giovanni Celiberto. Vector Quarkonia at the LHC with Jethad: A High-Energy Viewpoint. *Universe*, 9(7):324, 2023.
4. Emilien Chapon et al. Prospects for quarkonium studies at the high-luminosity LHC. *Prog. Part. Nucl. Phys.*, 122:103906, 2022.
5. Martin Hentschinski and Emilio Padrón Molina. Exclusive J/Ψ and $\Psi(2s)$ photo-production as a probe of QCD low x evolution equations. *Phys. Rev. D*, 103(7):074008, 2021.
6. A. Arroyo Garcia, M. Hentschinski, and K. Kutak. QCD evolution based evidence for the onset of gluon saturation in exclusive photo-production of vector mesons. *Phys. Lett. B*, 795:569–575, 2019.
7. I. Bautista, A. Fernandez Tellez, and Martin Hentschinski. BFKL evolution and the growth with energy of exclusive J/ψ and Υ photoproduction cross sections. *Phys. Rev. D*, 94(5):054002, 2016.
8. Martin Hentschinski. The use of QCD evolution to detect gluon saturation in exclusive photo-production of vector mesons. In *Workshop of QCD and Forward Physics at the the LHC, the future Electron Ion Collider and Cosmic Ray Physics*, pages 187–192, Lawrence, 2020. University of Kansas Libraries.
9. Martin Hentschinski. QCD evolution based evidence for the onset of gluon saturation in exclusive photo-production of vector mesons. *PoS*, EPS-HEP2019:528, 2020.
10. Martin Hentschinski and Krzysztof Kutak. Signs for the onset of gluon saturation in exclusive photo-production of vector mesons. *PoS*, LHCP2019:039, 2019.
11. Martin Hentschinski. The growth with energy of vector meson photo-production cross-sections and low x evolution. *PoS*, DIS2017:054, 2018.
12. Martin Hentschinski, Agustín Sabio Vera, and Clara Salas. Hard to Soft Pomeron Transition in Small- x Deep Inelastic Scattering Data Using Optimal Renormalization. *Phys. Rev. Lett.*, 110(4):041601, 2013.
13. Martin Hentschinski, Agustín Sabio Vera, and Clara Salas. F_2 and F_L at small x using a collinearly improved BFKL resummation. *Phys. Rev. D*, 87(7):076005, 2013.
14. Grigorios Chachamis, Michal Deák, Martin Hentschinski, Germán Rodrigo, and Agustín Sabio Vera. Single bottom quark production in k-factorisation. *Journal of High Energy Physics*, 2015(9):1–17, 2015.

15. Krzysztof Kutak and Sebastian Sapeta. Gluon saturation in dijet production in p-Pb collisions at Large Hadron Collider. *Phys. Rev. D*, 86:094043, 2012.
16. J. Nemchik, Nikolai N. Nikolaev, E. Predazzi, B. G. Zakharov, and V. R. Zoller. The Diffraction cone for exclusive vector meson production in deep inelastic scattering. *J. Exp. Theor. Phys.*, 86:1054–1073, 1998.
17. Jan Cepila, Jan Nemchik, Michal Krelina, and Roman Pasechnik. Theoretical uncertainties in exclusive electroproduction of s-wave heavy quarkonia. *The European Physical Journal C*, 79:1–29, 2019.
18. Krzysztof J. Golec-Biernat and M. Wusthoff. Saturation effects in deep inelastic scattering at low Q^2 and its implications on diffraction. *Phys. Rev. D*, 59:014017, 1998.
19. Shreyasi Acharya et al. Energy dependence of coherent photonuclear production of J/ψ mesons in ultra-peripheral Pb-Pb collisions at $\sqrt{s_{NN}}=5.02$ TeV. 5 2023.
20. Shreyasi Acharya et al. First measurement of the $|t|$ -dependence of incoherent J/ψ photonuclear production. 5 2023.
21. Marco Alcazar Peredo and Martin Hentschinski. Ratio of J/Ψ and $\Psi(2s)$ exclusive photoproduction cross sections as an indicator for the presence of nonlinear QCD evolution. *Phys. Rev. D*, 109(1):014032, 2024.
22. Marco Antonio Alcazar Peredo and Martin Hentschinski. Exclusive Photo-production of J/Ψ and $\Psi(2s)$ as a tool to explore the transition to high and saturated gluon densities at the LHC. *Rev. Mex. Fis. Suppl.*, 4(2):021121, 2023.
23. S. Acharya, D. Adamová, et al. First measurement of the $-\ln|t|$ -dependence of coherent j/ψ photonuclear production. *Physics Letters B*, 817:136280, 2021.
24. Michal Krelina, Jan Nemchik, Roman Pasechnik, and Jan Cepila. Spin rotation effects in diffractive electroproduction of heavy quarkonia. *Eur. Phys. J. C*, 79(2):154, 2019.
25. Stanley J. Brodsky, Tao Huang, and G.Peter Lepage. The Hadronic Wave Function in Quantum Chromodynamics. 6 1980.
26. Néstor Armesto and Amir H. Rezaeian. Exclusive vector meson production at high energies and gluon saturation. *Phys. Rev. D*, 90(5):054003, 2014.
27. L. Frankfurt, A. Radyushkin, and M. Strikman. Interaction of small size wave packet with hadron target. *Phys. Rev. D*, 55:98–104, 1997.
28. J. Bartels, K. Golec-Biernat, and H. Kowalski. Modification of the saturation model: Dokshitzer-gribov-lipatov-altarelli-parisi evolution. *Phys. Rev. D*, 66:014001, Jun 2002.
29. Krzysztof Golec-Biernat and Sebastian Sapeta. Saturation model of DIS : an update. *JHEP*, 03:102, 2018.
30. S. Chekanov et al. Exclusive electroproduction of J/ψ mesons at HERA. *Nucl. Phys. B*, 695:3–37, 2004.
31. C. Alexa et al. Elastic and Proton-Dissociative Photoproduction of J/ψ Mesons at HERA. *Eur. Phys. J. C*, 73(6):2466, 2013.
32. A. Aktas et al. Elastic J/ψ production at HERA. *Eur. Phys. J. C*, 46:585–603, 2006.
33. Betty Bezverkhny Abelev et al. Exclusive J/ψ photoproduction off protons in ultra-peripheral p-Pb collisions at $\sqrt{s_{NN}} = 5.02$ TeV. *Phys. Rev. Lett.*, 113(23):232504, 2014.
34. Shreyasi Acharya et al. Energy dependence of exclusive J/ψ photoproduction off protons in ultra-peripheral p-Pb collisions at $\sqrt{s_{NN}} = 5.02$ TeV. *Eur. Phys. J. C*, 79(5):402, 2019.
35. Exclusive and dissociative J/ψ photoproduction, and exclusive dimuon production, in p-Pb collisions at $\sqrt{s_{NN}} = 8.16$ TeV. 4 2023.
36. R Aaij et al. Exclusive J/ψ and $\psi(2S)$ production in pp collisions at $\sqrt{s} = 7$ TeV. *J. Phys. G*, 40:045001, 2013.
37. Roel Aaij et al. Central exclusive production of J/ψ and $\psi(2S)$ mesons in pp collisions at $\sqrt{s} = 13$ TeV. *JHEP*, 10:167, 2018.
38. D. Schmidt. *Diffractive photoproduction of charmonium in the H1 detector at HERA*. PhD thesis, Hamburg U., 2001.
39. C. Adloff et al. Diffractive photoproduction of $\psi(2S)$ mesons at HERA. *Phys. Lett. B*, 541:251–264, 2002.
40. Armen Tumasyan et al. Probing Small Bjorken-x Nuclear Gluonic Structure via Coherent J/ψ Photoproduction in Ultraperipheral Pb-Pb Collisions at $s_{NN}=5.02$ TeV. *Phys. Rev. Lett.*, 131(26):262301, 2023.
41. A. M. Stasto, Krzysztof J. Golec-Biernat, and J. Kwiecinski. Geometric scaling for the total $\gamma^* p$ cross-section in the low x region. *Phys. Rev. Lett.*, 86:596–599, 2001.

42. A. H. Mueller and S. Munier. Rapidity gap distribution in diffractive deep-inelastic scattering and parton genealogy. *Phys. Rev. D*, 98(3):034021, 2018.
43. A. H. Mueller and D. N. Triantafyllopoulos. The Energy dependence of the saturation momentum. *Nucl. Phys. B*, 640:331–350, 2002.
44. S. Munier and Robert B. Peschanski. Traveling wave fronts and the transition to saturation. *Phys. Rev. D*, 69:034008, 2004.
45. S. Munier and Robert B. Peschanski. Geometric scaling as traveling waves. *Phys. Rev. Lett.*, 91:232001, 2003.
46. I. Abt et al. Measurement of the cross-section ratio $\sigma_{(2S)}/\sigma_{J/\psi(1S)}$ in exclusive photoproduction at HERA. *JHEP*, 12:164, 2022.
47. C. Adloff et al. Diffractive photoproduction of $\psi(2S)$ mesons at HERA. *Phys. Lett. B*, 541:251–264, 2002.